Soft Matter

PAPER

View Article Online
View Journal



Cite this: DOI: 10.1039/c4sm02321h

# On polydispersity and the hard sphere glass transition

Emanuela Zaccarelli,*[a] Siobhan M. Liddle[b] and Wilson C. K. Poon[b]

Received 22nd October 2014
Accepted 12th November 2014

DOI: 10.1039/c4sm02321h

www.rsc.org/softmatter

We investigate the dynamics of polydisperse hard spheres at high packing fractions $\phi$. We use extensive numerical simulations based on an experimentally-realistic particle size distribution (PSD) and compare to commonly-used PSDs such as Gaussian or top hat distribution. We find that the mode of kinetic arrest depends on the PSD's shape and not only on its variance. For the experimentally-realistic PSD we find ageing dynamics even though the density correlators decay fully to zero for $\phi \geq 0.59$. We observe substantial decoupling of the dynamics of the smallest and largest particles. While the smallest particles remain diffusive in all our simulations, a power-law describes the largest-particle diffusion, suggesting an ideal arrest at $\phi_c \sim 0.588$. The latter is however averted just before $\phi_c$, due to the presence of the mobile smallest particles. In addition, we identify that a partial aging mechanism is at work, whose effects are most pronounced for the largest particles. By comparing our results with recent experimental observations of ergodic behavior up to $\phi \sim 0.6$ in a hard-sphere system, we argue that this is an effect of polydispersity, which smears out the glass transition.

## Introduction

Despite many decades of experimental, theoretical and simulational effort, the glass transition remains only partially understood. The discovery in the 1980s that hard-sphere-like, sterically-stabilised polymethylmethacrylate (PMMA) colloids underwent kinetic arrest[1] at a packing fraction of $\phi = \phi_g \approx 0.58$ opened up a fruitful avenue of investigation, because many features of such kinetic arrest in colloids can be mapped onto analogues in atomic and molecular glasses. In particular, hard sphere colloids have become a favourite test bed for mode coupling theory (MCT).[2,3] Apart from over-estimating the tendency to vitrify ($\phi_g^{MCT} \approx 0.52$), MCT gives a quantitative account of the main features on approach to arrest, such as a two-step decay in the system's intermediate scattering function (ISF) and power-law dependence of transport coefficients on $|\phi - \phi_g|$.[4]

Such correspondence notwithstanding, doubts remain as to whether hard spheres really do undergo a glass transition at $\phi_g \approx 0.58$. Some point to the ease with which monodisperse hard spheres at $\phi \geq 0.58$ crystallise in simulations[5] and in microgravity[6] to suggest that terrestrial arrest is due to the inevitable presence in real samples of size polydispersity ($s =$ the standard deviation of the size divided by the mean). However, recent simulations[8,9] show that particle dynamics near $\phi \approx 0.58$ is nearly invariant for $s \leq 8\%$. Thus, both polydisperse and monodisperse hard spheres form glasses, only that the latter are poor glass formers and crystallise easily.[10,11]

Others suggest that the ideal glass transition in hard spheres is preempted by activated processes[7] not taken into account by MCT. A recent study[12] appears to support this view. Measurements of the ISF of PMMA colloids over 7 decades in time show that the system remains ergodic at $\phi \geq 0.59$ reinforcing the view that activated processes delay the glass transition well beyond MCT; indeed, the suggestion is that there is perhaps no arrest before random close packing $\phi_{rcp} \approx 0.64$.

The work of Brambilla *et al.*[12] has generated significant controversy. Some pointed out their data were largely compatible with MCT if uncertainties in measuring $\phi$[13] were taken into account,[14] while others suggested that the large polydispersity ($s > 0.10$) used in ref. 12 to avoid crystallisation could be responsible for the supposed regime of activated dynamics.[15] The authors of ref. 12 subsequently simulated polydisperse hard spheres with a top hat particle size distribution (PSD) and reported relaxation times compatible with experiments, concluding that polydispersity was not relevant for their findings.[16,17] The issue stands unresolved. Its clarification is crucial, since hard spheres have been a favourite model for glass theory for the last 30 years.

We have performed extensive simulations of glassy arrest in concentrated, polydisperse hard spheres with PSDs of several shapes, including a PSD measured experimentally by transmission electron microscopy (TEM) for polydisperse PMMA colloids very similar to those used by Brambilla *et al.*[17] The distribution is highly skewed to the left with an extended tail of

[a]CNR-ISC Uos Sapienza and Dipartimento di Fisica, Sapienza Università di Roma, P.le A. Moro 2, I-00185, Roma, Italy. E-mail: emanuela.zaccarelli@phys.uniroma1.it
[b]SUPA, School of Physics and Astronomy, University of Edinburgh, Mayfield Road, Edinburgh, EH9 3JZ, Scotland

small particles, and can be described by a Weibull distribution.[18] Consistent with ref. 12, we find that the ISFs decay to zero at $\phi = 0.59$ and beyond. However, these ISFs depend on the waiting time, *i.e.* they age. In this regime, the dynamics of the smallest and largest particles are decoupled, similar to what occurs in asymmetric binary mixtures[19–24] where it is possible for only the larger species to arrest. In our case, the diffusion coefficient of the largest particles $D_l$ follows a power law consistent with ideal arrest at $\phi_c \sim 0.588$, until very close to $\phi_c$, the non-ergodicity catastrophe is averted due to the smaller particles, which remain mobile. Such heterogeneous dynamics is also reflected in an unusual partial aging behaviour, which is most pronounced for the large particles. This peculiar dynamics is not the result of activated dynamics, but a manifestation of polydispersity, which smears out the glass transition. Hence, instead of a transition point, we observe a region of points where the system behaves with mixed characteristics of both liquid and glass, due to the more liquid/glass character of small/large particles coexisting in the system.

## Methods

We perform event-driven Molecular Dynamics (MD) simulations of hard spheres with different PSDs. Crucially, this includes a PSD obtained experimentally from PMMA particles synthesised in-house, which were very similar to those used in ref. 12. The experimental PSD, Fig. 1, was measured from TEM (Phillips CM120 Biotwin) at $\times$2850, at which the mean particle diameter $\langle\sigma\rangle \approx 40$ pixels. Averaging over $\approx$2200 particles gave $\langle\sigma\rangle = 248 \pm 4$ nm and $s = 12 \pm 1\%$. A Weibull fit well describes the experimental data, Fig. 1.

We simulate $N = 2309$ particles with the experimental PSD, including measurement noise in order to have the most realistic possible representation of the system, Fig. 1 inset. We define large and small tail populations as particles with sizes $>(1+\alpha)\langle\sigma\rangle$ and $<(1-\alpha)\langle\sigma\rangle$ respectively. The choice of $\alpha$ does not qualitatively affect our findings. We use $\alpha = 0.1$ to give optimal statistics for the tail populations, which consist of $\sim$400 particles each. The unclassified majority $\left(\sim\frac{2}{3}\right)$ constitute the 'average' particles. The large and small populations have average size ratio 1.13 and 0.8 (with a 1.41 ratio between the two), but extreme size ratios as large as 3 exist in this PSD. For comparison, we also consider $N = 2000$ particles taken from Gaussian and top hat distributions with the same $\langle\sigma\rangle$ and $s$ as the experimental PSD; the top hat spans sizes in the range $0.8\langle\sigma\rangle$ to $1.2\langle\sigma\rangle$, and its variance is 11.5%.[16] We use units in which the particle mass $m = 1$, average diameter $\bar{\sigma} = 1$, thermal energy $k_BT = 1$ and time is measured in $\bar{\sigma}(m/k_BT)^{0.5}$.

In all simulations, we first equilibrate the system in the NVT ensemble and then production runs are monitored in the microcanonical ensemble. From the long-time limit of the mean-squared displacement (MSD) the average self-diffusion coefficient $D$ is obtained. Averages are performed over different subsets of particles for calculating the small $D_s$ and large $D_l$ diffusivities. At high $\phi$, we monitor aging and distinguish state points showing clear waiting time dependence from equilibrium ones. For this purpose, data collected using the experimental PSD for $\phi \geq 0.59$ have been averaged over ten independent runs. In these cases, the waiting time $t_w$ is defined as the start of the NVT run. We calculate the self and collective ISFs at the first peak of the static structure factor and extract corresponding relaxation times, respectively $\tau^{self}$ and $\tau$, where the ISF is at $e^{-1}$. We also calculate the partial relaxation times for both types of correlators, *i.e.* $\tau_s^{self}$ and $\tau_s$ for small particles, $\tau_l^{self}$ and $\tau_l$ for large ones.

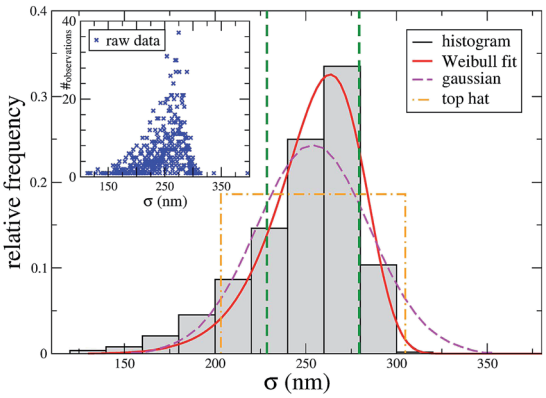


Fig. 1 Size distribution measured from TEM (histogram) and fitted Weibull distribution (continuous red curve). The average diameter and polydispersity are $\langle\sigma_{TEM}\rangle = 248$ nm and $s_{TEM} = 12\%$ respectively, while the Weibull fit gives $\langle\sigma_W\rangle = 254$ nm and $s_W = 10\%$. Populations of small and large particles are defined as those differing from the average diameter by more than 10% (left and right of dashed verticals). Also shown are the Gaussian (dashed magenta curve) and top hat (dot-dashed orange curve) PSD with the same polydispersity. The latter have been normalised to have equal area to the experimental PSD. Inset: raw data of PSD as they were used in the simulations.

## Results

### Dependence on $\phi$ of the dynamics for the experimental PSD

The self and collective ISFs calculated for the experimental PSD are shown in Fig. 2(a) as a function of time for different values of $\phi$. While for $\phi < 0.59$ data fully decay to zero and do not show aging features, the ISFs at larger $\phi \geq 0.59$ show aging dependence. Thus, data in Fig. 2(a) for $\phi \geq 0.59$ are obtained averaging over independent configurations at a fixed waiting time $t_w$. Although the curves do not decay fully to zero within our simulation window, they show a clear tendency to depart from the plateau at long times, suggesting that they would eventually decay to zero in longer simulations. *Prima facia*, a fully-decaying ISF indicates an equilibrated liquid, unless specific aging effects are present. In our case, we observe clear aging in the $\phi \geq 0.59$ data. We thus consider these state points as 'aging liquids'. The ISF of this 'aging liquid' fully decays to zero, but on a progressively longer time scale as waiting time advances. Usually such behaviour eventually leads to arrest, even on extremely long timescales, one dramatic example being that of Laponite clay suspensions.[26] In the present case, however, there is no evidence (see also below) that the system will eventually arrest, despite continuing to age.

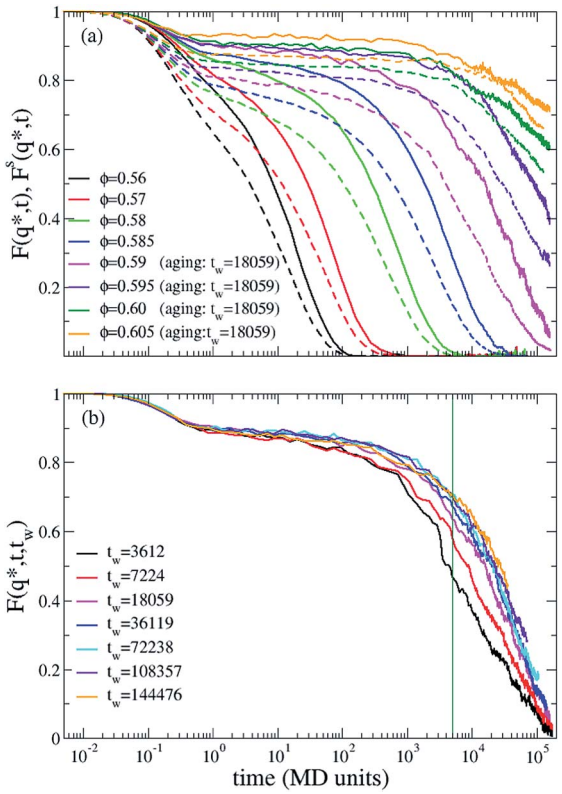


Fig. 2 (a) Self (dashed lines) and collective (full lines) ISFs, calculated at the peak of static structure factor $q^*$, as a function of $\phi$. Data for $\phi \geq 0.59$ are taken at $t_w = 18\,059$ and averaged over 10 independent runs; (b) collective ISF as a function of $t_w$ at $\phi = 0.59$. The vertical line demarcates the time window up to which the ISF has reached stationarity, indicating a clear departure from the plateau and suggesting restoration of ergodicity at extremely long times.

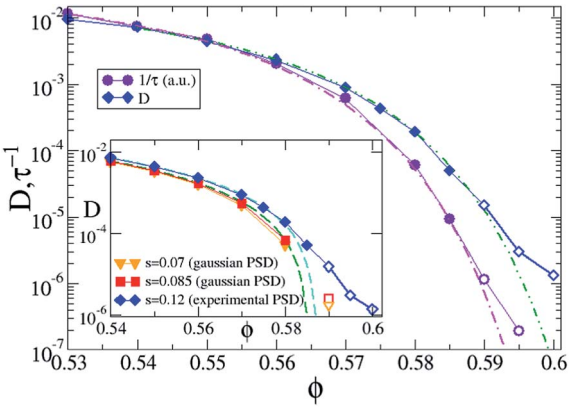


Fig. 3 Self-diffusion coefficient $D$ and inverse collective relaxation time $\tau^{-1}$ (scaled by factor 1/40) as a function of $\phi$ for the experimental PSD. Fits with $\exp[-C/(\phi_g - \phi)^\delta]$ (dot-dashed and double-dot-dashed lines) give $\phi_g = 0.635 \pm 0.005$ and $\delta = 2.3 \pm 0.1$ for both observables. The fits describe data well up to $\phi = 0.59$, which is at the onset of aging behaviour. Closed (open) symbols represent equilibrium (aging) state points. Data for $\phi \geq 0.59$ can only be considered an upper bound of the real $D$, $\tau^{-1}$. Inset: $D$ as a function of $\phi$ for the experimental PSD with $s = 0.12$ and for Gaussian PSD with smaller $s$ taken from ref. 8. The dashed lines are power-law fits to the data for $s = 0.08$ ($\gamma \sim 2.3$ and $\phi_g \sim 0.585$) and $s = 0.12$ ($\gamma \sim 2.1$ and $\phi_g \sim 0.587$) respectively.

In Fig. 2(b) the waiting time dependence of the ISF for $\phi = 0.59$ is reported, showing that aging persists even after waiting a transient comparable to the relaxation time (*e.g.* $t_w \sim 10^5$). We notice that this aging behaviour is subtly different from what observed in conventional aging of glasses.[27,28] Indeed, at the longest studied $t_w$, the correlators do reach a stationary state for times below 5000 (see vertical line in Fig. 2(b)), where it is clear that still a clear departure from the plateau persists. While we cannot at present extend our simulation time window to the timescale of experiments performed by Brambilla and coworkers,[12] we are still able to observe that the ultimate fate of the system for $\phi \sim 0.59$ is that of a fluid, albeit with extremely long equilibration times.

The relaxation times $\tau$ are plotted as a function of $\phi$ together with the self-diffusion coefficient $D$ in Fig. 3. Both sets of data are well described by an exponential singularity $D$, $\tau^{-1} \sim \exp[1/(\phi - \phi_g)^\delta]$, where $\phi_g \approx \phi_{rcp}$ in both cases and $\delta \approx 2.3$–$2.4$, suggesting an approximate double exponential singularity in good agreement with results of Brambilla *et al.*[12] In the inset, we compare $D$ for the experimental PSD with $s = 0.12$ (as in the main panel) with previous results for Gaussian PSDs with $s = 0.07$ and 0.085,[8] Fig. 3. Unlike when $0 < s \leq 0.08$,[8] the dynamics speed up with $s$.[25] More interestingly, we find that the shape of $D(\phi)$ changes upon increasing $s$. For $s \leq 0.08$, $D \sim |\phi - \phi_g|^\gamma$ with $\gamma \sim 2.2$–$2.3$ and $\phi_g \sim 0.585$, consistent with an MCT glass transition,[8] with aging in states above $\phi_g \sim 0.585$. On the other hand for $s = 0.12$, the decrease of $D(\phi)$ becomes much less pronounced at high $\phi$ and a power-law behavior fails to account of all fluid state points. Thus, some fundamental difference exists between almost monodisperse hard spheres ($s \leq 0.08$) and polydisperse ones ($s = 0.12$), which changes the dependence of transport coefficients on packing fraction and provides clear deviations from simple MCT predictions (based on a monodisperse system).

## Decoupling of dynamics of smallest and largest particles and partial aging

To better understand what is going on in our polydisperse system, we consider $D$ for the tails of the experimental PSD, Fig. 4. From the beginning of our investigated range, $\phi = 0.52$, there is a clear dynamical separation between the smallest and largest sub-populations, which increases with $\phi$, reaching $D_s \sim 10^2 D_l$ at $\phi = 0.59$. This observation is reminiscent of binary asymmetric mixtures[19–24] in which the small particles remain mobile in a matrix of arrested large ones. In our case, we find that $D_\ell \sim |\phi - \phi_c|^\gamma$ with $\phi_c \sim 0.588$ and $\gamma \sim 2.3$ fits all our results up to and including the data point at $\phi = 0.585$. Thus, the largest sub-population behaves as if it is heading towards an ideal hard-sphere glass transition at $\phi_c$. However, deviations are observed thereafter, with a measurably finite value of $D$ at $\phi = 0.59$ (although suffering of aging effects).

A putative non-ergodicity catastrophe of the largest sub-population is therefore averted, presumably because of the presence of smaller particles. In particular, our data show that

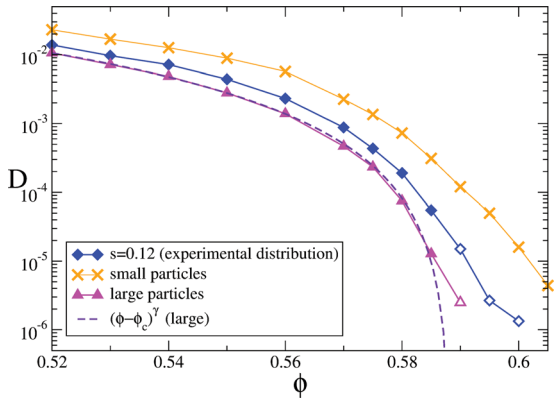


Fig. 4 Average and partial self-diffusion coefficients (respectively $D_l$ and $D_s$ for large and small particles) as a function of $\phi$ for the experimental PSD. A power-law fit (dashed line) with $\gamma \sim 2.3$ and $\phi_c \sim 0.588$ describes well $D_l$, while small particles remain mobile at all investigated $\phi$.

the smallest sub-population remains clearly mobile up to $\phi = 0.605$; moreover, $D_s(\phi)$ cannot be fitted to a power law suggestive of arrest at any higher $\phi$. The smearing of a true glass transition by the presence of the small, mobile particles produces an intriguing state with mixed characteristics of liquids and glasses, with large and small sub-populations showing quite distinct dynamics. Thus it is the presence of residual diffusivity in the small particles that generates the unusual aging dynamics of the systems beyond what would be normally considered as glassy regime in monodisperse or slightly polydisperse hard spheres.

In addition to the decay of the ISF found even for large $t_w$, discussed earlier and shown in Fig. 2(b), we also find evidence of a clear partial aging. Fig. 5 shows the aging dependence of the partial MSD of small and large particles for $\phi = 0.595$. It is evident that the small particles MSD easily reach its long-time

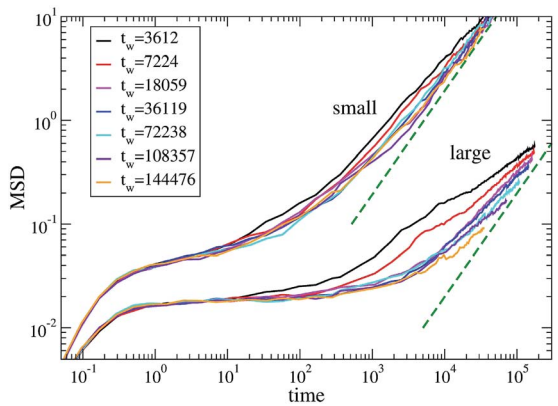


Fig. 5 Mean squared displacement (MSD) for small and large particles as a function of waiting times at $\phi = 0.595$. Data are averaged over ten independent configurations. Dashed lines (in green) show diffusive behaviour. An unusual partial aging behaviour is observed: small particles after a transient equilibrate and reach long-time diffusion, which is independent of $t_w$; large particles instead show clear aging and always remain sub-diffusive.

diffusion behaviour and do not age any more at large enough $t_w$. On the other hand, large particles MSD continues to age and most importantly it remains subdiffusive at long times. This, previously unreported, partial aging is a direct consequence of the heterogeneous dynamics in the system that is caused by the large polydispersity.

## Heterogeneous dynamics

Interestingly, the decoupling between large and small sub-populations is much less obvious in the $\phi$-dependence of the partial relaxation times. Indeed, from the decoupling of the diffusivities of these sub-populations one may have expected the same for the partial self relaxation times. However, studies of binary mixtures have shown that a full decoupling between self and collective dynamics only occurs for size ratios ≥5 (ref. 21 and 29) or for a sufficient fraction of large particles,[20] neither of which is the case in our experimental PSD. Hence, we find that the variation of $D_s/D_l$ with $\phi$ exceeds that of $\tau_l^{self}/\tau_s^{self}$ by roughly one order of magnitude, Fig. 6(a). As $D_l$ begins to drop precipitously relative to $D_s$ at high $\phi$, $\tau_l^{self}$ fails to rise in proportional relative to its 'small' counterpart, $\tau_s^{self}$. If we take $\tau^{self}$ as a surrogate for viscosity, then the lack of scaling between $D$ and $\tau^{self}$ can be seen as a manifestation of the violation of the Stokes–Einstein relation (SER). SER violation is ubiquitous in atomic and molecular glass formers,[30,31] where the product $D\tau$ increases on approaching the glass transition. This is commonly interpreted as evidence for increasing spatial heterogeneities in the dynamics. In our case, there is a far sharper rise in $D_s\tau_s^{self}$ with $\phi$ than in $D_l\tau_l^{self}$. This indicates a high degree of dynamic heterogeneity for the small sub-population.

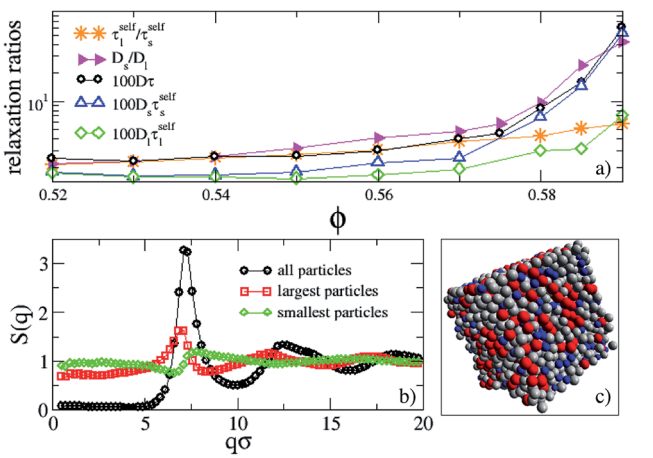


Fig. 6 (a) Ratios of large and small particles transport coefficients as a function of $\phi$. Note that $D\tau$, $D_s\tau_s^{self}$ and $D_l\tau_l^{self}$ have been multiplied by a factor 100 to put data on the same scale; (b) total and partial static structure factors at $\phi = 0.59$. Data are averaged over different independent runs. The partial structure factors have been scaled by the concentration of the respective species; (c) snapshot of the system at $\phi = 0.60$. Particles are represented with their own size and have been classified according to different colours: small particles in blue, large particles in red and intermediate-sized particles in grey. The small particles can be seen as moving in a random, porous matrix of larger particles.

A close inspection of partial structure factors Fig. 6(b) reveals that large and small particles are randomly distributed. There is indeed no preferential ordering of the particles according to their size and particles are disordered and homogeneously distributed even among the different subsets. This is clear also from visualising a snapshot of the system, shown in Fig. 6(c), where large and small particles (in red and blue respectively) are randomly distributed in the simulation box. Hence, the large particles form an almost arrested random matrix in which small particles diffuse, providing a conceptual link of our system to fluids in a porous matrix[32–34] (although here the large particles eventually still manage to regain ergodicity thanks to the role of the small ones). This link is reinforced by the finding of a high degree of dynamic heterogeneity in the small particles, similarly to what has been observed for mobile particles diffusing in a porous matrix.[35]

### Dependence of dynamics on the PSD shape

It is important to ask how the features that we have observed for the experimental PSD depend on the distribution, specifically, whether any dependence is mostly determined by $s$, or by the PSD's whole shape. We therefore repeat the simulations using a Gaussian distribution with $s = 0.12$ and a top hat distribution with $s = 0.115$, Fig. 1. Fig. 7(a) shows that, averaged over the whole system, $D(\phi)$ is essentially independent of the shape of the PSD, but depends only on its variance. Fig. 7(b) also shows that lowering $s$ decreases the difference between $D_s$ and $D_l$. Thus, the low-$s$ colloids used by Pusey and van Megen[1,4,28] should still show ideal arrest of all particles simultaneously at $\phi \sim 0.58$–$0.59$ without any effect of partial localisation.

However, we find that important differences emerge between the top hat and the other two PSDs at comparable $s$ when we analyse the contributions from small and large particles, plotted in Fig. 7(b), as the diffusivity ratio $D_l/D_s$. While $D_l/D_s \sim 10^{-2}$ at $\phi = 0.59$ for the experimental PSD, it is $\approx 5$ times larger for the top-hat PSD, for which selective localisation of the larger particles is a much weaker effect. Presumably, this is because defining sub-populations of small and large particles makes little sense in a uniform distribution compared to the same exercise in strongly-peaked PSDs. Indeed, at high $\phi$ the residual diffusivity detected also in the top-hat PSD is still due to a gradation of dynamics, from slower, larger particles to faster, smaller particles, although this is not as extreme as for the experimentally realistic PSD. Fig. 8(a) shows this in two ways. In the main figure, we compare the diffusivities of the particles in the smallest and largest bin in a 10-bin division of the top-hat distribution as a function of $\phi$. The inset shows the mean squared displacements (MSD) as a function of time for all 10 bins at $\phi = 0.58$. Note that all these bins have equal populations, weighting equally on the average of the total $D$, resulting in a smearing of differences that are, by contrast, enhanced by the presence of peaks and tails in more realistic PSDs.

Moreover, a power law fit, associated to an MCT-type ideal glass transition, does not equally well describe the behavior of the large sub-population in the top-hat PSD. Fig. 8(b) compares $D_l(\phi)$ for the experimental and top-hat PSDs defined using $\alpha = 0.1$. As we have already shown in the main text, $D_\ell \sim |\phi - \phi_c|^\gamma$ with $\phi_c \sim 0.588$ and $\gamma \sim 2.3$ describes the experimental PSD data well for all but the last data point, which showed ageing and

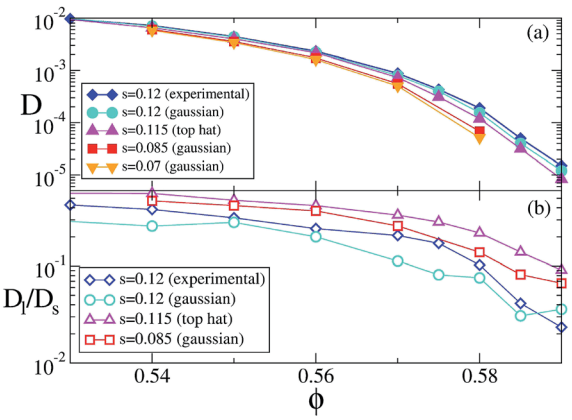


Fig. 7 (a) Average self diffusion coefficient and (b) ratio of the large to small diffusivity as functions of $\phi$ for different PSD shapes as described in the labels.

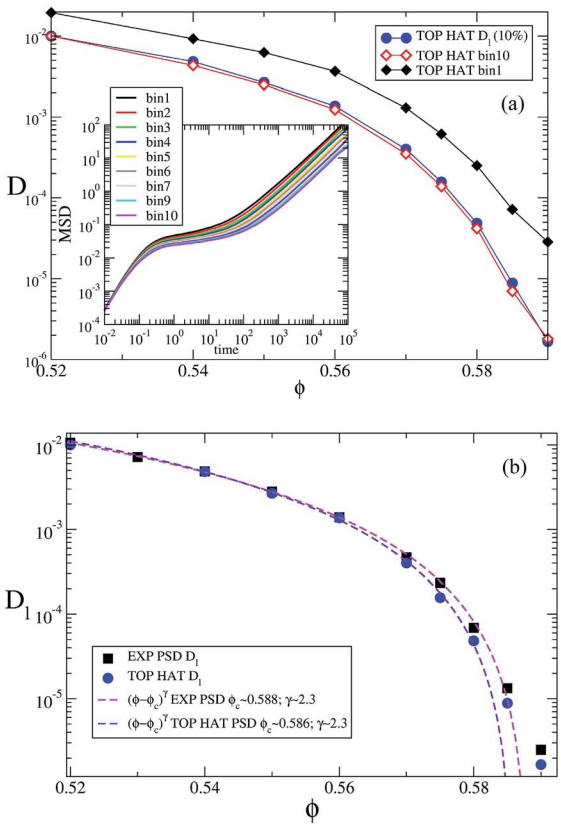


Fig. 8 Diffusion coefficients of the large particles $D_l$ for the top hat distribution: (a) comparison with those calculated in a 10-bin analysis of the distributions. Bin1 contains the smallest particles, while bin10 contains the largest ones; (b) power-law fit and comparison with the experimental PSD. Applying a power-law fit to the top-hat data yields an anticipated transition at $\phi_c \sim 0.586$, which clearly misses the last equilibrium data point in the simulations. Inset of (a): MSD *versus* time for the particles in different bins at $\phi = 058$.

therefore must be above any putative $\phi_c$. Fitting the same functional form to the top-hat data returns the same $\gamma$, but a transition point of $\phi_c \sim 0.586$. The measured $D_l$ for the top-hat PSD at this $\phi$ is substantial, and the system at this $\phi$ does not show ageing.

Thus, we conclude that we cannot identify a putative ideal (a la MCT) arrest transition of the sub-population of large particles for the top-hat PSD. This conclusion is insensitive to the precise definition of 'large'. Fig. 8(a) also compares the $D_l(\phi)$ data for the top-hat PSD with those calculated for the particles in the largest bin in a classification of the top-hat PSD into 10 equal bins. There is no material difference in the results. Thus, we conclude that a uniform distribution with the same $s$ as the experimental PSD does not reproduce key qualitative features of the microscopic dynamics of the latter, while the use of a (peaked) Gaussian PSD does largely reproduce these features, especially at $\phi \geq 0.58$, Fig. 7(b). Interestingly, there is residual diffusivity in all three PSDs at $\phi \geq 0.59$.

### Comparison with experimental data in ref. 16

In this section we perform a direct comparison of the collective relaxation time $\tau$ calculated from the simulations with the experimental one measured by Brambilla *et al.*[12,16] Despite the different microscopic dynamics between experiments (Brownian) and simulations (Newtonian), we build on previous works which have shown that the long-time slow dynamics is independent of the microscopic one.[36,37] Experimental and numerical results are compared in Fig. 9. To superimpose the numerical data onto the experimental ones, we use a double shift factor which takes into account the uncertainty of the packing fraction (on the $x$-axis)[13] and the difference in microscopic time (on the $y$-axis). In this way, we obtain a scaling factor of 1.011 for $\phi_{exp}$ in terms of $\phi$, which gives an estimate of the experimental error on determining $\phi$ of the order of 1%. Therefore, we find that $\phi_{exp} = 0.5876, 0.5953, 0.5970, 0.5990$ are equivalent respectively to $\phi \sim 0.5812, 0.5888, 0.5905, 0.5925$ in our simulations. Also, 1 MD time unit = 0.0075 s real time, so that our longest waiting time is $\sim 10^3$ s.

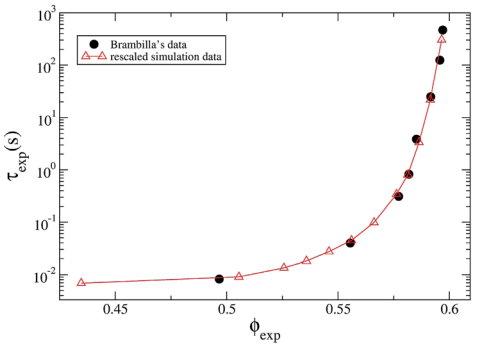


Fig. 9 Relaxation times from simulations of the experimental PSD, obtained from the collective ISF at the peak of the static structure factor, compared with data taken from.[16] In both cases the relaxation time is the time where the ISF reaches $e^{-1}$. The numerical data have been scaled as: $1.011\phi = \phi_{exp}$ and $\tau/0.0075 = \tau_{exp}$.

Based on this comparison, we now discuss the ageing behaviour observed by Brambilla *et al.* in ref. 16. In this work, the authors claim to observe usual ageing behaviour up to the experimental $\phi_{exp} = 0.5990$ ($\phi = 0.5925$). However, the equilibration time of their sample at $\phi_{exp} = 0.5876$ ($\phi = 0.5812$) is larger by a factor of 30 than the relaxation time. This may suggest that the system is at the limit of equilibration. For densities $\phi_{exp} = 0.5953, 0.5970$ ($\phi = 0.5888, 0.5905$), a small drift is observed at long times for $\tau$ *vs.* $t_w$ (see Fig. 6 of ref. 16). If we compare the aging behaviour in the simulations (Fig. 2(b) of the manuscript) at $\phi = 0.59$ with that for the corresponding experimental samples, we have that the maximum waiting time in the simulations is $\sim 10^3$ s. This is considerably smaller than the experimental waiting times and one can see, again in Fig. 6 of ref. 16, that the system is still (moderately) aging at this time. Although on longer and longer timescales, $t = 10^4$ to $10^5$ s, the system may indeed be considered equilibrated, it is clear that this timescale is much larger than the $\alpha$-relaxation time ($O(10^3)$), so that something non-trivial happens around $\phi \sim 0.59$ also in the experimental system in terms of the system dynamics, in agreement with what observed in our simulations. While many factors can alter the equilibration time in experiments, such as shaking or thermalisation, we are tempted to speculate that the long time required for the system to 'equilibrate' is the result of the decoupling of the dynamics between large and small particles. Indeed, a complete equilibration is achieved when also the largest particles have relaxed from their initial state, which takes a time much larger than the average time. We suggest that this generates the unusual ageing observed in the simulations, and is therefore an effect intrinsic to the wide polydispersity of the system.

## Conclusions

We have shown that polydispersity has highly non-trivial effects on the hard sphere glass transition. In particular, we find that experimentally realistic, peaked PSDs preempt the occurrence of an ideal glass transition at $\phi \sim 0.58$, and give rise to an unusual aging behaviour due to a strong decoupling between small and large particles in the tails of the PSD. Within our simulation window, the large particles tend to, but never quite reach, arrest, while the small particles remain essentially diffusive, providing a way to avoid non-ergodicity to the system. Indeed the correlators still fully decay to zero for $\phi \geq 0.59$, despite showing aging effects.

It appears that a system with a peaked PSD is conceptually close to a binary mixture in which MCT predicts a localisation transition of only the largest particles. We do not fully observe this behaviour in our system – $D_\ell(\phi)$ deviates from power-law behavior near $\phi_c$ – because the size differential between large and small sub-populations is not sufficiently extreme. It is probable that such a system will eventually arrest into a conventional glassy state at higher $\phi$ than those reached in this work. Thus, the glass transition is smeared out from a sharp point to a region where aging seem to coexist with ergodicity. Such behaviour is due to the presence of large, quasi-glassy particles and small, very mobile particles characterised by

 

partial aging. Thus it is an effect of polydispersity, rather than the signature of activated processes.

Our findings are compatible with the view that moderately polydisperse hard spheres, $s \sim 5$–6%, can function as a reference system for glassy arrest. On the other hand, hard spheres with larger polydispersity, $s \geq 0.10$, at large packing fractions, $\phi \geq 0.59$, behave in a far more complex way, where several particle populations, some with large dynamic heterogeneities, are present and cannot therefore be used directly as a model to test simple theories of the glass transition. Since in the simulations we cannot probe at present the long-time scales explored in the experiments, it would be desirable then to repeat the experiments performed in ref. 12 for particles with lower polydispersities to really see whether deviations from MCT continue to be observed. For the more polydisperse ones, the great level of complexity of the system makes it difficult to move beyond the descriptive understanding given in this work to elucidate the microscopic mechanisms[38] operative in such systems; this will be addressed in future work.

## Acknowledgements

We thank A. Schofield for particles, and L. Cipelletti, S. Egelhaaf, M. Laurati, V. Martinez, E. Sanz, C. Valeriani, T. Voigtmann for discussions. We acknowledge support from ITN-234810-COMPLOIDS. EZ acknowledges support from MIUR-FIRB ANISOFT (RBFR125H0M). SML was funded by an EPSRC studentship. WCKP and part of EZ's visit to Edinburgh were funded by EPSRC grant EP/J007404/1. TEM was performed in the Wellcome Trust Centre (UoE). Simulations were performed using resources provided by the Edinburgh Compute and Data Facility (ECDF) (http://www.ecdf.ed.ac.uk/).

## References

1 P. N. Pusey and W. van Megen, *Nature*, 1986, **320**, 340.
2 U. Bengtzelius, W. Götze and A. Sjölander, *J. Phys. C: Solid State Phys.*, 1984, **17**, 5915.
3 W. Götze, in *Liquids, Freezing and the Glass Transition*, ed. J.-P. Hansen, D. Levesque and J. Zinn-Justin, Elsevier, Amsterdam, 1991, p. 287.
4 W. van Megen, T. C. Mortensen, S. R. Williams and J. Muller, *Phys. Rev. E: Stat. Phys., Plasmas, Fluids, Relat. Interdiscip. Top.*, 1998, **58**, 6073.
5 M. D. Rintoul and S. Torquato, *Phys. Rev. Lett.*, 1996, **77**, 4198.
6 J. Zhu, M. Li, R. Rogers, W. Meyer, R. H. Ottewill, W. B. Russell and P. M. Chaikin, *Nature*, 1997, **387**, 883.
7 G. Szamel and E. Fenner, *Europhys. Lett.*, 2004, **67**, 779.
8 E. Zaccarelli, C. Valeriani, E. Sanz, W. C. K. Poon, M. E. Cates and P. N. Pusey, *Phys. Rev. Lett.*, 2009, **103**, 135704.
9 P. N. Pusey, E. Zaccarelli, C. Valeriani, E. Sanz, W. C. K. Poon and M. E. Cates, *Philos. Trans. R. Soc., A*, 2009, **367**, 4993.
10 M. Fasolo and P. Sollich, *Phys. Rev. Lett.*, 2003, **91**, 68301.
11 P. Sollich and N. Wilding, *Phys. Rev. Lett.*, 2010, **104**, 118302.
12 G. Brambilla, D. El Masri, M. Pierno, L. Berthier, L. Cipelletti, G. Petekidis and A. B. Schofield, *Phys. Rev. Lett.*, 2009, **102**, 085703.
13 W. C. K. Poon, E. R. Weeks and C. P. Royall, *Soft Matter*, 2012, **8**, 21.
14 J. Reinhardt, F. Weysser and M. Fuchs Phys, *Phys. Rev. Lett.*, 2010, **105**, 199604.
15 W. van Megen and S. R. Williams, *Phys. Rev. Lett.*, 2010, **104**, 169601.
16 D. El Masri, G. Brambilla, M. Pierno, G. Petekidis, A. B. Schofield, L. Berthier and L. Cipelletti, *J. Stat. Mech.: Theory Exp.*, 2009, P07015.
17 G. Brambilla, D. El Masri, M. Pierno, L. Berthier, L. Cipelletti, G. Petekidis and A. B. Schofield, *Phys. Rev. Lett.*, 2010, **104**, 169602.
18 G. Bryant, S. Martin, A. Budi and W. van Megen, *Langmuir*, 2003, **19**, 616.
19 A. Imhof and J. K. G. Dhont, *Phys. Rev. Lett.*, 1995, **75**, 1662.
20 T. Voigtmann and J. Horbach, *Europhys. Lett.*, 2006, **74**, 459.
21 T. Voigtmann and J. Horbach, *Phys. Rev. Lett.*, 2009, **103**, 205901.
22 A. J. Moreno and J. Colmenero, *Phys. Rev. E: Stat., Nonlinear, Soft Matter Phys.*, 2006, **74**, 021409.
23 C. Mayer, F. Sciortino, C. N. Likos, P. Tartaglia, H. Loewen and E. Zaccarelli, *Macromolecules*, 2009, **42**, 423.
24 T. Voigtmann, *EPL*, 2011, **96**, 36006.
25 R. P. Sear, *J. Chem. Phys.*, 2000, **113**, 4732.
26 B. Ruzicka, L. Zulian and G. Ruocco, *Phys. Rev. Lett.*, 2004, **93**, 258301.
27 W. Kob and J.-L. Barrat, *Phys. Rev. Lett.*, 1997, **78**, 4581.
28 V. A. Martinez, G. Bryant and W. van Megen, *J. Chem. Phys.*, 2010, **133**, 114906.
29 A. J. Moreno and J. Colmenero, *J. Chem. Phys.*, 2006, **125**, 164507.
30 F. Fujara, B. Geil, H. Sillescu and G. Fleischer, *Z. Phys. B: Condens. Matter*, 1992, **88**, 195.
31 M. T. Cicerone and M. D. Ediger, *J. Chem. Phys.*, 1996, **104**, 7210.
32 V. Krakoviack, *Phys. Rev. Lett.*, 2005, **94**, 065703; *Phys. Rev. E: Stat., Nonlinear, Soft Matter Phys.*, 2007, **75**, 031503.
33 J. Kurzidim, D. Coslovich and G. Kahl, *Phys. Rev. Lett.*, 2009, **103**, 138303.
34 K. Kim, K. Miyazaki and S. Saito, *EPL*, 2009, **88**, 36002.
35 J. Kurzidim, D. Coslovich and G. Kahl, *J. Phys.: Condens. Matter*, 2011, **23**, 234122.
36 T. Gleim, W. Kob and K. Binder, *Phys. Rev. Lett.*, 1998, **81**, 4404.
37 A. M. Puertas, E. Zaccarelli and F. Sciortino, *J. Phys.: Condens. Matter*, 2005, **17**, L271–L278.
38 E. Sanz, C. Valeriani, E. Zaccarelli, W. C. K. Poon, M. Cates and P. N. Pusey, *PNAS*, 2014, **111**, 75.